Available online at www.sciencedirect.com
SCIENCE DIRECT®
International Journal of Solids and Structures 43 (2006) 4578–4594
INTERNATIONAL JOURNAL OF SOLIDS and STRUCTURES
www.elsevier.com/locate/ijsolstr

Development mechanism of local plastic buckling in bars subjected to axial impact

Anwen Wang *, Wenying Tian

Teaching and Research Section of Material Mechanics, P.O. Box 0116, The Naval Academy of Engineering, Wuhan 430033, PR China

Received 16 March 2005; received in revised form 30 June 2005
Available online 30 August 2005

Abstract

In order to clarify the developmental mechanism of the local plastic buckling and the interaction between axial wave and buckling deformation in an axially impacted slender-bar, the non-linear dynamic equations in the incremental form are derived and solved by use of the finite difference method, with the axial wave front treated as a moving boundary. The initial local-buckling deflection given by the characteristic-value analysis is used as the initial condition of the solution of the equations, instead of the initial imperfection that is assumed in literatures. It is found that the initial buckling deflection with one half-wave, occurring near the impacted end, develops into the higher post-buckling mode with several half-waves, as the axial compression waves propagate forward. The numerical results show that no strain reversal occurs at the early stage of post-buckling process, and the solution corresponding to the tangent-modulus theory is valid for the dynamic plastic post-buckling response of the bar at this stage. The theoretical results are in good agreement with the experimental results reported in the literature.
© 2005 Elsevier Ltd. All rights reserved.

Keywords: Non-linear dynamics; Axial impact; Plastic dynamic buckling; Local buckling development; Twin characteristic parameter

1. Introduction

The plastic buckling problem of straight bars subjected to an axial dynamic loading has been studied extensively (Abrahamson and Goodier, 1966; Hayashi and Sano, 1972a; Lee, 1981; Lindberg and Florence, 1983; Simitses, 1987, 1989; Jones, 1989; Karagiozova and Jones, 1996; Lepik, 2001). For this problem, the earlier analyses usually assumed that the bar is instantaneously brought to the state of uniform compression

* Corresponding author. Tel.: +86 (0)2783648269.
E-mail address: wtng4509@public.wh.hb.cn (A. Wang).

0020-7683/$ - see front matter © 2005 Elsevier Ltd. All rights reserved.
doi:10.1016/j.ijsolstr.2005.06.091

stress (Hayashi and Sano, 1972a; Lindberg and Florence, 1983). Recently, Karagiozova and Jones (1996), and Lepik (2001) investigated, respectively, the influence of stress wave propagation on the elastic-plastic dynamic buckling of the bar under axial impact.

In the analysis for the non-linear dynamic response of the buckling bar, it is usually assumed that the unstressed bar has an initial imperfection, in the shape of a half sine wave, distributed along the entire bar (Hayashi and Sano, 1972a,b). In the calculation of integrating the motion equations, the imperfection is used as the initial condition of the solution of the equations. However, the test results (Hayashi and Sano, 1972b) of axial impact buckling for the slender bar show that, when the impact velocity is high, the local buckling occurs near the impact end at an early stage of the impact process. The same situation is illustrated by a sequence of high speed photographs for the dynamic buckling of an aluminum alloy strip under axial impact (Lindberg and Florence, 1983; see Fig. 2.15 in Lindberg and Florence, 1983).

In Wang and Tian (2002, 2003a,b, 2005), the twin-characteristic-parameter method was presented to clarify the mechanism of buckling initiation and obtain the critical conditions for the geometrically perfect bar as well as the cylindrical shell subjected to an axial dynamic loading. From the analysis by use of the twin-characteristic-parameter method, it is found that, when a geometrically perfect slender-bar is subjected to the axial impact with a high velocity, an initial local-buckling will occur, near the impact end, at the early stage of the process for the axial compression wave to propagate, from the impact end, towards another end of the bar. Assuming that the process of the impact for the bar is initiated at the instant $t = 0$, we define the instant $i = t_{cr}$, at which an infinitesimal buckling deflection occurs near the impact end, as the critical buckling instant. In the duration from $t = 0$ to $t = t_{cr}$, the axial compression wave has traveled the distance L_{cr} in the bar.We define L_{cr} as the critical buckling length. At the critical instant $t = t_{cr}$, the infinitesimal buckling deflection is limited to the region of the length L_{cr} near the impact end, and the part of the bar before the front of the compression wave remains undisturbed. The critical buckling instant t_{cr} and the mode of the infinitesimal buckling deflection can be obtained from the analysis for the critical state by use of twin-characteristic-parameter method (Wang and Tian, 2002, 2003a, in press).

In order to clarify the developmental mechanism of the local buckling deformation in the axially impacted slender-bar, it is quite natural that the initial local-buckling deflection is used as the initial condition of the solution for the dynamic post-buckling response, instead of the initial imperfection distributed along the entire bar. In this way, the elastic dynamic post-buckling response of the slender bar subjected to the axial impact was investigated (Wang and Tian, in press). The theoretical results are in good agreement with the experimental results reported (Lindberg and Florence, 1983; Hayashi and Sano, 1972b) respectively. For the aluminum alloy strip (Lindberg and Florence, 1983), the length of the first half-wave of the post-buckling mode, predicted by the theoretical analysis of Wang and Tian (in press), is equal to 11.2 mm, and is close to the experimental value of 11.9 mm given by Lindberg and Florence (1983). For the Ni–Cr steel bar impacted axially by a striking mass with the velocity $v_0 = 6.3$ m/s, the analysis of Wang and Tian (in press) gives that, at the post-buckling stage, the maximum bending moment appears at the position $x/L = 0.05238$, where L is the length of the bar and x the axial coordinate. In comparison, the experimental result of Hayashi and Sano (1972b) is that $x/L = 0.05$.

In this paper, in order to clarify the developmental mechanism of the local plastic buckling and the interaction between axial wave and buckling deformation in the bar subjected to the axial impact against a rigid wall, the non-linear dynamic equations in the incremental form are derived and solved by use of the finite difference method, with the axial wave front treated as a moving boundary. The initial plastic buckling mode with a small amplitude parameter, obtained by use of the twin-characteristic-parameter solution, is applied as the initial condition of the solution of the non-linear dynamic equations.

In the present analysis, it is assume that the bar is made of the linear strain-hardening material. The tangent-modulus theory and the double-modulus theory are applied, respectively, for describing the relation between the bending-moment and curvature in the dynamic plastic post-buckling deformation. In the relation between the axial stress-increment and strain-increment, both the loading case due to compressive-

wave propagation and the unloading case induced by the buckling deformation are taken into account. The validity of the theory is examined carefully by the numerical investigation. The numerical results show that no strain reversal occurs at the early stage of post-buckling process, and the solution corresponding to the tangent-modulus theory is valid for the dynamic plastic post-buckling response of the bar at this stage. The theoretical results are in good agreement with the experimental results reported by Lindberg and Florence (1983).

2. Initial compression wave in the bar impacted against a rigid wall

As shown in Fig. 1, the straight bar with the length L is originally stress-free and moving, at the velocity v_0, toward a rigid wall. On impact the left end of the bar immediately come to rest. When the stress at the cross-section of the impacted end exceeds the yield stress σ_s of the material, a plastic compression wave as well as an elastic compression wave is produced by the impact. The elastic and plastic waves travels towards the free end of the bar, at the velocities c_0 and c_1 respectively. It is assumed that the bar is made of the linear strain-hardening material, of which Young's modulus is E, the strain-hardening modulus E_t and the density ρ. The elastic wave velocity c_0 and the plastic wave velocity c_1 are calculated by use of the following equations, respectively.

$$c_0 = \sqrt{\frac{E}{\rho}}, \quad c_1 = \sqrt{\frac{E_t}{\rho}} \tag{2.1}$$

Assuming that the process of the impact is initiated at the instant $t = 0$, after a small interval t the elastic wave and the plastic wave have passed the distances L_e and L_p respectively in the bar.

$$L_e = c_0 t, \quad L_p = c_1 t \tag{2.2}$$

At this stage, L_e is a small quantity in comparison with the value of the length L of the bar, and no buckling deformation takes place in the bar. The axial strain of the bar, produced by the axial compression waves, can be approximately calculated according to the following equations:

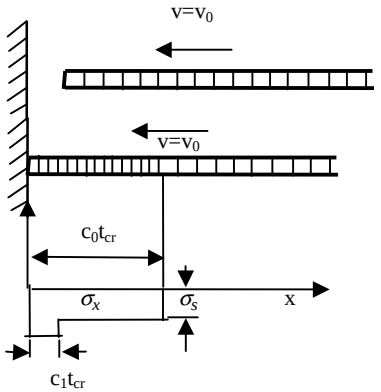

Fig. 1. Axial stress in the bar at the initial stage of impact.

$$\begin{aligned}
\varepsilon_x &= -\frac{v_0}{c_1} + \left(\sqrt{\frac{E}{E_t}} - 1\right)\frac{\sigma_s}{E} \quad (0 < x < c_1 t) \\
\varepsilon_x &= -\frac{\sigma_s}{E} \quad (c_1 t < x < c_0 t) \\
\varepsilon_x &= 0 \quad (c_0 t < x < L)
\end{aligned} \tag{2.3a–c}$$

The corresponding axial stress at the cross-section of the bar is expressed as

$$\begin{aligned}
\sigma_x^{(1)} &= -E_t\frac{v_0}{c_1} - \left(1 - \sqrt{\frac{E_t}{E}}\right)\sigma_s \quad (0 < x < c_1 t) \\
\sigma_x^{(2)} &= -\sigma_s \quad (c_1 t < x < c_0 t) \\
\sigma_x^{(3)} &= 0 \quad (c_0 t < x < L)
\end{aligned} \tag{2.4a–c}$$

In Eqs. (2.4a–c), the superscripts (1), (2) and (3) in the stress symbol σ_x are corresponding to the three regions $0 < x < c_1 t$, $c_1 t < x < c_0 t$, and $c_0 t < x < L$, respectively.

3. Critical buckling time and initial buckling mode

As shown in Fig. 1, the bar is subjected to the axial impact against the rigid wall, and the elastic and plastic compression waves are produced by the impact. If the bar is slender, an infinitesimal initial buckling deflection will occur at the early stage of the process for the compression waves to propagate towards the free end of the bar. The critical length L_{cr}, to which the infinitesimal initial buckling deflection is confined, is equal to the length of the part covered by the elastic compression wave at the critical instant $t = t_{\mathrm{cr}}$, that is, $L_{\mathrm{cr}} = c_0 t_{\mathrm{cr}}$. At the instant $t = t_{\mathrm{cr}}$, the part of the bar, before the front of the elastic compression wave, remains undisturbed.

When the impact velocity v_0 is given, the axial stress in the bar is calculated by use of Eqs. (2.4a–c). From Eq. (5.4) in Wang and Tian (2003a), the expressions for the critical length L_{cr} and the critical time t_{cr} are written as

$$L_{\mathrm{cr}} = \pi \cdot r \cdot \sqrt{\frac{\Lambda\overline{E}}{\left|\sigma_x^{(1)}\right|}}, \quad t_{\mathrm{cr}} = \frac{L_{\mathrm{cr}}}{c_0} \tag{3.1a, b}$$

In Eq. (3.1a), r is the gyration radius of the cross-section of the bar and Λ denotes the critical load parameter. On the assumption that no strain reversal occurs in the process of buckling initiation, $\overline{E}$ is equal to the strain-hardening modulus E_t, which is corresponding to the tangent-modulus theory. When the double-modulus theory is applied to the analysis, $\overline{E}$ is taken as the reduced modulus E_r (Bleich, 1952).

The critical load parameter Λ, the inertial exponential-parameter Ω in the following Eq. (3.3), and the initial dynamic buckling modes are calculated by the characteristic-value analysis presented in Wang and Tian (2003a) for the plastic dynamic buckling of the straight bar. In the analysis of Wang and Tian (2003a), it is assumed that the loaded end of the bar is simply supported in the buckling process. According the buckling deformation of specimens in the experiment (see Fig. 2.23; Lindberg and Florence, 1983), in the present analysis we assume that, in the process of buckling occurrence, the impact end of the bar remains perpendicular to the surface of the rigid wall and there is no slide between the impact end and the rigid wall. In this case, the clamp condition is applied to the impact end, that is,

$$\bar{w}_0(\xi,\tau)|_{\xi=0,\tau=1}=0,\quad \bar{w}_{0,\xi}|_{\xi=0,\tau=1}=0 \tag{3.2}$$

The lowest values of the parameters Λ, Ω and the critical buckling time t_{cr} are related to the first dynamic buckling mode. From the solution of Wang and Tian (2003a), the expression of the dimensionless initial buckling deflection $\bar{w}_0$ corresponding to the first dynamic buckling mode is written as:

$$\bar{w}_0=\frac{w_0}{r}=\eta\cdot e^{\bar{c}_1\bar{r}\Omega(\tau-1)}Y(x) \tag{3.3}$$

In Eq. (3.3), η is the small amplitude parameter, and other parameters are defined as follows:

$$\bar{c}_1=\frac{c_1}{c_0},\quad \bar{r}=\frac{r}{L_{cr}},\quad \tau=\frac{t}{t_{cr}} \tag{3.4a–c}$$

From Eqs. (4.3) and (4.4) in Wang and Tian (2003a), the expressions of $Y(x)$ are written as

$$\begin{aligned} Y(x)&=D_1\cos(\beta_1 x)+D_2\sin(\beta_1 x)+D_2\cos(\beta_2 x)+D_4\sin(\beta_2 x)\quad (0\leqslant x\leqslant c_1 t_{cr})\\ Y(x)&=C_1\cos(\chi_1 x)+C_2\sin(\chi_1 x)+C_3\cos(\chi_2 x)+C_4\sin(\chi_2 x)\quad (c_1 t_{cr}\leqslant x\leqslant c_0 t_{cr}) \end{aligned} \tag{3.5a, b}$$

where, the values of the parameters β_1, β_2, χ_1 and χ_2 are related to the characteristic parameters Λ and Ω in terms of the Eqs. (4.5), (4.6) and (5.3b) in Wang and Tian (2003a), and the parameters D_1, D_2, D_3, D_4, C_1, C_2, C_3 and C_4 are a set of eight integration constants.

The dynamic buckling mode (3.3) must satisfy the two boundary conditions of Eqs. (3.2a,b) at the impact end, four continuity conditions at the front of the plastic compression wave, two boundary conditions at the front of the elastic compression wave, and one supplementary restraint condition obtained from the criterion of energy conservation in the process of the dynamic buckling initiation (Wang and Tian, 2003a) (see Eqs. (2.17a–d), (2.15a,b) and (3.17) in Wang and Tian (2003a), respectively). For the supplementary restraint condition at compression wave fronts, more careful derivation by use of Eq. (3.14) in Wang and Tian (2003a) gives the equations:

$$c_1\cdot[\sigma_{x0}^{(1)}-\sigma_{x0}^{(2)}]\varepsilon_{x1}|_{x=c_1 t}+\frac{1}{2}\bar{E}r^2c_0\cdot[w_{0,xx}^2]_{x=c_0 t}=0 \tag{3.6}$$

In Eq. (3.6), ε_{x1} is the increment of the axial strain due to buckling deformation. Assuming that no axial unloading occurs in the transient process of buckling initiation, from Eq. (3.6) we obtain

$$\varepsilon_{x1}|_{x=c_1 t}=0,\quad w_{0,xx}|_{x=c_0 t}=0 \tag{3.7a, b}$$

In the present analysis we use the supplementary restraint condition (3.7b) instead of Eq. (3.17) in Wang and Tian (2003a). The numerical results of examples in the Section 5 of this paper show that difference caused by this change is small and negligible. By use of the nine restraint conditions as mentioned above, seven of the eight integration constants D_1, D_2, D_3, D_4, C_1, C_2, C_3 and C_4, and the characteristic parameters Λ and Ω can be calculated.

By use of Eqs. (2.3a–c), the axial displacement u_0 of the central line of the bar, at the critical instant $t=t_{cr}$, is written as follows:

$$\begin{aligned} u_0&=\left[\left(\sqrt{\frac{E}{E_t}}-1\right)\frac{\sigma_s}{E}-\frac{v_0}{c_1}\right]\cdot x\quad \text{for } 0\leqslant x\leqslant c_1 t_{cr}\\ u_0&=\left[\left(\sqrt{\frac{E}{E_t}}-1\right)\frac{\sigma_s}{E}-\frac{v_0}{c_1}\right]\cdot c_1 t_{cr}-\frac{\sigma_s}{E}(x-c_1 t_{cr})\quad \text{for } c_1 t_{cr}\leqslant x\leqslant c_0 t_{cr}\\ u_0&=-v_0 t_{cr}\quad \text{for } c_0 t_{cr}\leqslant x\leqslant L \end{aligned} \tag{3.8a–c}$$

4. Dynamic post-buckling equations and their difference solution

4.1. The dynamic post-buckling equations of the bar

If an initial local buckling occurs near the impact end of the bar at the early stage of the process for the elastic and plastic compression waves to propagate towards the free end, the buckling deformation will develop with the propagation of the compression waves. To simplify the theoretical treatment, the present analysis is limited to the post-buckling stage at which the elastic compression wave has not arrived at the free end of the bar. For the slender bar, the effects of shear deformation and rotary inertia are negligible, and the non-linear dynamic equations of the buckling bar are written as

$$\sigma_{x,x} - \rho u_{,tt} = 0 \tag{4.1}$$

$$M_{x,xx} - A(\sigma_x w_{,x})_{,x} + \rho A w_{,tt} = 0 \quad \text{for } 0 \leqslant x \leqslant c_0 t \tag{4.2}$$

where σ_x denotes the average axial stress at the cross-section of the bar in the region $0 \leqslant x \leqslant c_0 t$, M_x is the bending moment, u denotes the total axial-displacement of the center line of the bar after the buckling, and w is the lateral displacement corresponding to the buckling deformation. The symbol $(_{,x})$ and $(_{,t})$ denote differentiation with the coordinate x and the time variable t respectively.

Let (u^t, w^t) denote the displacements at the instant t, and $(u^{t+\Delta t}, w^{t+\Delta t})$ denote the displacements at the instant $t + \Delta t$, where Δt denotes the small increment of the time variable t. From the instant t to the instant $t + \Delta t$, the axial strain increment $\Delta\varepsilon_x$ of the central line is expressed as

$$\Delta\varepsilon_x = u^{t+\Delta t}_{,x} - u^t_{,x} + \frac{1}{2}\left(w^{t+\Delta t}_{,x}\right)^2 - \frac{1}{2}\left(w^t_{,x}\right)^2 \tag{4.3}$$

Then, the dynamic equations (4.1) and (4.2) at the instant $t + \Delta t$ are written in the forms:

$$\sigma^t_{x,x} + \tilde{E}\left[u^{t+\Delta t}_{,x} - u^t_{,x} + \frac{1}{2}(w^{t+\Delta t}_{,x})^2 - \frac{1}{2}(w^t_{,x})^2\right]_{,x} = \rho u^{t+\Delta t}_{,tt} \tag{4.4a}$$

$$\overline{E} I w^{t+\Delta t}_{,xxxx} - A\left\{\left[\sigma^t_x + \tilde{E}\left(u^{t+\Delta t}_{,x} - u^t_{,x} + \frac{1}{2}\left(w^{t+\Delta t}_{,x}\right)^2 - \frac{1}{2}\left(w^t_{,x}\right)^2\right)\right] w^{t+\Delta t}_{,x}\right\}_{,x} + \rho A w^{t+\Delta t}_{,tt} = 0$$

$$\text{for } 0 \leqslant x \leqslant c_0(t + \Delta t) \tag{4.4b}$$

Eqs. (4.4a,b) is the system of two non-linear dynamic equations with a moving boundary at the elastic compression-wave front, where A is the cross-sectional area of the bar, and I the moment of inertia of the cross-section. The theory on the dynamic plastic post-buckling is very complicated. To simplify the theoretical treatment, in literatures it is usually assumed that the axial strain rate dominates the extensional strain rate introduced by the bending motion, therefore, no strain-rate reversal occurs until the buckling deformation has developed enough (Hayashi and Sano, 1972a; Lindberg and Florence, 1983). On the above-mentioned assumption, the modulus $\overline{E}$ in Eq. (4.4b) is identical with the strain-hardening modulus E_t. In this case, $\overline{E}$ in Eq. (3.1a) is also taken as the modulus E_t, that is, the tangent-modulus theory is applied to the calculation of the critical length L_{cr} and the critical time t_{cr}. When the double-modulus theory is applied to the calculation of L_{cr} and t_{cr} in Eqs. (3.1a,b), $\overline{E}$ in Eq. (4.4b) is taken as the reduced modulus E_r (Bleich, 1952).

The modulus $\tilde{E}$ in Eqs. (4.4a,b) is determined in accordance with the following expressions:

$$\begin{aligned}
&\tilde{E} = E \quad \text{if } \Delta\varepsilon_x > 0 \\
&\tilde{E} = E_t \quad \text{if } \Delta\varepsilon_x < 0 \quad \text{and} \quad |\sigma^t_x| \geqslant \sigma_s \\
&\tilde{E} = E \quad \text{if } \Delta\varepsilon_x < 0,\ |\sigma^t_x| < \sigma_s \quad \text{and} \quad |\sigma^t_x + E \cdot \Delta\varepsilon_x| \leqslant \sigma_s \\
&\tilde{E} = E_t - \left(1 - \frac{E_t}{E}\right)\frac{\sigma^t_x + \sigma_s}{\Delta\varepsilon_x} \quad \text{if } \Delta\varepsilon_x < 0, |\sigma^t_x| < \sigma_s \quad \text{and} \quad |\sigma^t_x + E \cdot \Delta\varepsilon_x| > \sigma_s
\end{aligned} \tag{4.5a–d}$$

In Eqs. (4.5a–d), the elastic and plastic loading of the axial stress, due to the propagation of the compression waves towards the free end, and the elastic unloading of the axial stress caused by the buckling deformation are taken into account. The symbol || denotes the absolute value of the corresponding quantity. For the convenience of analysis, we introduce the following dimensionless quantities and variables:

$$\bar{u}=\frac{L_{\mathrm{cr}}}{r}\frac{u}{r},\quad \bar{w}=\frac{w}{r},\quad \bar{\sigma}_x^t=\left(\frac{L_{\mathrm{cr}}}{r}\right)^2\frac{\sigma_x^t}{E},\quad \xi=\frac{x}{L_{\mathrm{cr}}},\quad \tau=\frac{t}{t_{\mathrm{cr}}}, \tag{4.6a–e}$$

where t_{cr}, is the critical buckling time, and L_{cr} the critical buckling length: $L_{\mathrm{cr}}=c_0t_{\mathrm{cr}}$. With Eqs. (4.6a–e) introduced, the governing equations (4.4a,b) are written into the dimensionless forms:

$$\bar{\sigma}_{x,\xi}^t+\frac{\tilde{E}}{E}\left[\bar{u}_{,\xi}^{t+\Delta t}-\bar{u}_{,\xi}^t+\frac{1}{2}\left(\bar{w}_{,\xi}^{t+\Delta t}\right)^2-\frac{1}{2}\left(\bar{w}_{,\xi}^t\right)^2\right]_{,\xi}-\bar{u}_{,\tau\tau}^{t+\Delta t}=0$$

$$\bar{w}_{,\xi\xi\xi\xi}^{t+\Delta t}-\alpha\left\{\left[\bar{\sigma}_x^t+\kappa\left(\bar{u}_{,\xi}^{t+\Delta t}-\bar{u}_{,\xi}^t+\frac{1}{2}\left(\bar{w}_{,\xi}^{t+\Delta t}\right)^2-\frac{1}{2}(\bar{w}_{,\xi}^t)^2\right)\right]\bar{w}_{,\xi}^{t+\Delta t}\right\}_{,\xi}+\psi\bar{w}_{,\tau\tau}^{t+\Delta t}=0\qquad \text{for } 0\leqslant\xi\leqslant\tau+\Delta\tau \tag{4.7a, b}$$

where

$$\alpha=\frac{E}{\tilde{E}},\quad \kappa=\frac{\tilde{E}}{E},\quad \psi=\alpha\left(\frac{L_{\mathrm{cr}}}{r}\right)^2,\quad \Delta\tau=\frac{\Delta t}{t_{\mathrm{cr}}} \tag{4.8a–c}$$

The non-linear dynamic equations (4.7a,b) are solved by use of the difference method in the following section.

4.2. Initial conditions and boundary conditions for the solution of Eqs. (4.7a,b)

The axial displacement u_0 in Eqs. (3.8a–c) and the dimensionless initial buckling deflection $\bar{w}_0$ in Eq. (3.3) are used as the initial conditions, at the instant $t=t_{\mathrm{cr}}$ (that is, the instant $\tau=1$), for the solution of the dynamic post-buckling equations (4.7a,b), that is,

$$\bar{w}|_{\tau=1}=\bar{w}_0,\quad \bar{w}_{,\tau}|_{\tau=1}=\bar{w}_{0,\tau},\quad \text{for } 0\leqslant\xi\leqslant 1$$
$$\bar{w}|_{\tau=1}=0,\quad \bar{w}_{,\tau}|_{\tau=1}=0\quad \text{for } 1\leqslant\xi\leqslant L/L_{\mathrm{cr}} \tag{4.9a–c}$$

$$\bar{u}|_{\tau=1}=\frac{L_{\mathrm{cr}}}{r}\frac{u_0}{r}\quad \text{for } 0\leqslant\xi\leqslant L/L_{\mathrm{cr}} \tag{4.10}$$

The dimensionless axial stress $\bar{\sigma}_x^t$ at the critical instant $t=t_{\mathrm{cr}}$ is calculated by use Eqs. (2.4a–c) and (4.6c).

It is assumed that, at the impact stage before the separation of the impact end from the rigid wall, the impact end of the bar remains perpendicular to the surface of the rigid wall and there is no slide between the impact end and the rigid wall. In this case, the boundary conditions at the impact end are written as

$$\bar{u}(0,\tau)=0,\quad \bar{w}(0,\tau)=0,\quad \bar{w}_{,\xi}|_{\xi=0}=0 \tag{4.11}$$

As mentioned at the beginning of this section, the present analysis is limited to the post-buckling deformation stage at which the axial elastic wave has not arrived at the free end. The boundary conditions at the elastic compression wave front ($x=c_0(t+\Delta t)$ or $\xi=\tau+\Delta\tau$) are written as

$$\bar{u}(\xi,\tau)|_{\xi=\tau+\Delta\tau}=-\frac{v_0(\tau+\Delta\tau)}{c_0}\left(\frac{L_{\mathrm{cr}}}{r}\right)^2\quad \bar{w}(\xi,\tau)|_{\xi=\tau+\Delta\tau}=0,\qquad \bar{w}_{,\xi}\big|_{\xi=\tau+\Delta\tau}=0 \tag{4.12a–c}$$

4.3. The finite difference solution of Eqs. (4.7a,b)

The non-linear differential equations (4.7a,b) are solved by use of the finite difference method and the backward-difference formulas for the time variable τ are applied to the solution of the equations. In relation to the reference point $(\xi, \tau + \Delta\tau)$, as shown in Fig. 2, the difference expressions of the derivatives of the displacements $\bar{u}^{t+\Delta t}$ and $\bar{w}^{t+\Delta t}$ with respect to the variable τ or ξ, which appear in Eqs. (4.7a,b), are written as follows:

$$
\begin{aligned}
\bar{u}^{t+\Delta t}_{,\tau\tau} &= \frac{1}{(\Delta\tau)^2}[\bar{u}(\xi,\tau+\Delta\tau) - 2\bar{u}(\xi,\tau) + \bar{u}(\xi,\tau-\Delta\tau)] \\
\bar{w}^{t+\Delta t}_{,\tau\tau} &= \frac{1}{(\Delta\tau)^2}[\bar{w}(\xi,\tau+\Delta\tau) - 2\bar{w}(\xi,\tau) + \bar{w}(\xi,\tau-\Delta\tau)] \\
\bar{u}^{t+\Delta t}_{,\xi} &= \frac{1}{2\Delta\xi}[\bar{u}(\xi+\Delta\xi,\tau+\Delta\tau) - \bar{u}(\xi-\Delta\xi,\tau+\Delta\tau)] \\
\bar{u}^{t+\Delta t}_{,\xi\xi} &= \frac{1}{(\Delta\xi)^2}[\bar{u}(\xi+\Delta\xi,\tau+\Delta\tau) - 2\bar{u}(\xi,\tau+\Delta\tau) + \bar{u}(\xi-\Delta\xi,\tau+\Delta\tau)] \\
\bar{w}^{t+\Delta t}_{,\xi} &= \frac{1}{2\Delta\xi}[\bar{w}(\xi+\Delta\xi,\tau+\Delta\tau) - \bar{w}(\xi-\Delta\xi,\tau+\Delta\tau)] \\
\bar{w}^{t+\Delta t}_{,\xi\xi} &= \frac{1}{(\Delta\xi)^2}[\bar{w}(\xi+\Delta\xi,\tau+\Delta\tau) - 2\bar{w}(\xi,\tau+\Delta\tau) + \bar{w}(\xi-\Delta\xi,\tau+\Delta\tau)] \\
\bar{w}^{t+\Delta t}_{,\xi\xi\xi\xi} &= \frac{1}{(\Delta\xi)^4}[\bar{w}(\xi+2\Delta\xi,\tau+\Delta\tau) - 4\bar{w}(\xi+\Delta\xi,\tau+\Delta\tau) + 6\bar{w}(\xi,\tau+\Delta\tau) \\
&\quad -4\bar{w}(\xi-\Delta\xi,\tau+\Delta\tau) + \bar{w}(\xi-2\Delta\xi,\tau+\Delta\tau)]
\end{aligned}
\tag{4.13a–g}
$$

Similarly, the difference expressions of the derivatives of the displacements $\bar{u}^t$ and $\bar{w}^t$ with respect to the variable ξ, which appear in Eqs. (4.7a,b), are written as

$$
\begin{aligned}
\bar{u}^{t}_{,\xi} &= \frac{1}{2\Delta\xi}[\bar{u}(\xi+\Delta\xi,\tau) - \bar{u}(\xi-\Delta\xi,\tau)] \\
\bar{u}^{t}_{,\xi\xi} &= \frac{1}{(\Delta\xi)^2}[\bar{u}(\xi+\Delta\xi,\tau) - 2\bar{u}(\xi,\tau) + \bar{u}(\xi-\Delta\xi,\tau)] \\
\bar{w}^{t}_{,\xi} &= \frac{1}{2\Delta\xi}[\bar{w}(\xi+\Delta\xi,\tau) - \bar{w}(\xi-\Delta\xi,\tau)] \\
\bar{w}^{t}_{,\xi\xi} &= \frac{1}{(\Delta\xi)^2}[\bar{w}(\xi+\Delta\xi,\tau) - 2\bar{w}(\xi,\tau) + \bar{w}(\xi-\Delta\xi,\tau)]
\end{aligned}
\tag{4.14a–d}
$$

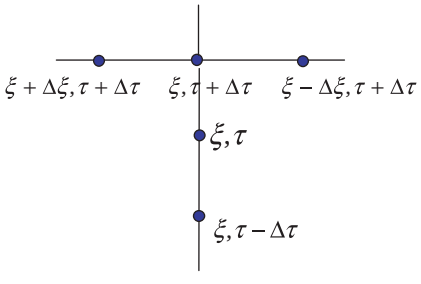

Fig. 2. Finite difference grid.

For the instant $t + \Delta t$ (that is, $\tau + \Delta\tau$), substituting the expressions (4.13a–g) and (4.14a–d) into Eqs. (4.7a,b) for every reference point $(\xi_i, \tau + \Delta\tau)$ gives a system of no-linear difference equations for the undetermined quantities $u^{t+\Delta t}(\xi_i, \tau + \Delta\tau)$ and $\bar{w}^{t+\Delta t}(\xi_i, \tau + \Delta\tau)$, where $i = 1, 2, \ldots$, including all grid points except the two points at the boundaries of the region $0 \leqslant \xi \leqslant \tau + \Delta\tau$. The iterative procedure is used to solve the no-linear equation system. The derivatives with respect to the variable ξ or τ in the above-mentioned boundary conditions and the initial conditions are also transformed into the corresponding difference formulas. In the calculation, we take $\Delta\xi = \Delta\tau$, that is, $\Delta x = c_0 \Delta t$, and the convergent numerical results are obtained.

5. Numerical results and discussion

Lindberg and Florence (1983) reported the plastic buckling experiment of 6061-T6 aluminum-alloy bars to be impacted against a heavy steel slab at the indicated velocities. For a set of bar specimens (Lindberg and Florence, 1983), the diameter of the cross-section is $d = 5.3$ mm and the length $L = 457$ mm. From the experimental data (Lindberg and Florence, 1983), the yield stress of the 6061–T6 aluminum alloy is $\sigma_s = 309$ MPa, Young's modulus $E = 67.5$ GPa, and the strain-hardening modulus $E_t = 1.24$ GPa. By use of the theory developed in Sections 2–4, we have investigated numerically the plastic dynamic buckling of six specimens, for which the values of the impact velocity v_0 given by Lindberg and Florence (1983) are list in Table 1.

In the calculation, the critical buckling time t_{cr} and the initial buckling mode $\bar{w}_0$ are computed by use of the formulas in Section 3, and the post-buckling displacements $\bar{u}$ and $\bar{w}$ are calculated according to the solution of Eqs. (4.7a,b). As mentioned in Sections 3 and 4.1, in Eqs. (3.1a) and (4.4b) $\overline{E}$ is taken as the strain-hardening modulus E_t for the tangent-modulus theory and the reduced modulus E_r for the double-modulus theory, respectively. Eqs. (4.5a–d) are applied to describing relation between the axial stress-increment and strain-increment, in which both the loading case due to the propagation of the compression waves and the unloading case caused by the buckling deformation are taken into account.

In Table 1, Λ is the critical load parameter, related to the first dynamic buckling mode, given by the characteristic-value analysis (Wang and Tian, 2003a). The critical length L^t_{cr} and the critical time t^t_{cr} are calculated from the tangent-modulus theory, and L^r_{cr} and t^r_{cr} from the double-modulus theory. In Table 1, $S_{t-\text{modulus}}$ denotes the length of the first half-wave, close to the impact end, in the post-buckling deflection profile at the instant $\tau = 11$, which is calculated by use of the tangent-modulus theory, and $S_{r-\text{modulus}}$ is the length of the first half-wave of the post-buckling deflection profile that is calculated by use of the double-modulus theory. The average values of the first two half-wave lengths, observed in the experiment of Lindberg and Florence (1983), are also listed in Table 1 and denoted by S_{exp}.

Table 1
Critical buckling length and half-wave length of post-buckling mode of impacted bars

Specimen.	v_0 (m/s)	Λ	L^t_{cr} (mm)	t^t_{cr} (10^{-6} s)	L^r_{cr} (mm)	t^r_{cr} (10^{-6} s)	Post-buckling half-wavelength (mm)		
							$S_{r-\text{modulus}}$	$S_{t-\text{modulus}}$	S_{exp} (Lindberg and Florence, 1983)
B1	104.3	13.03	24.73	4.95	43.55	8.71	28.99	15.80	16.26
B4	53.68	10.64	25.03	5.01	44.05	8.81	34.96	18.48	19.05
B14	52.16	10.60	25.07	5.01	44.16	8.83	35.18	18.55	19.81
B19	51.24	10.57	25.10	5.02	44.21	8.84	35.29	18.64	18.03
B15	44.84	10.40	25.30	5.06	44.57	8.91	36.11	19.09	18.80
B5	38.43	10.22	25.52	5.10	44.96	8.99	36.96	19.93	21.59

From the data in Table 1, it will be seen that the values of the critical buckling length and the post-buckling half-wavelength computed from the tangent-modulus theory are closer to the experimental results, in comparison with the values computed from the double-modulus theory. Therefore, in the following we discuss first the numerical results computed from the tangent-modulus theory, and then outline the results obtained from the double-modulus theory.

5.1. The numerical results computed from the tangent-modulus theory

The values of the critical length L_{cr}^{t} and the critical time t_{cr}^{t} related to the first dynamic buckling mode, computed from the tangent-modulus theory, are list in the fourth column and fifth column of Table 1, respectively. For the bar B4, $L_{cr}^{t} = 25.03$ mm, $t_{cr}^{t} = 5.01 \times 10^{-6}$ s, and the first dynamic buckling mode calculated by use of Eq. (3.3) is shown in Fig. 3, where the amplitude parameter $\bar{w}_0$ of is taken as $\eta = 0.01$. At the instant $t = 91.4 \times 10^{-6}$s, that is $\tau = t/t_{cr}^{t} = 18.24$, the elastic compression wave arrives at the free end. As mentioned previously, to simplify the analysis, in this paper the numerical investigation is limited to the dynamic post-buckling stage at which the elastic compression wave has not arrived the free end of the bar.

For the bar B4, the growth and spread of the post-buckling deflection w with the dimensionless time parameter τ is shown in Figs. 4 and 5 for $\eta = 0.01$. From Figs. 4 and 5, it will be seen that, in the process of the post-buckling deformation, the buckling deflection near the impact end spreads forward with the time and develops from the simplest mode with one half-wave into a series of higher post-buckling modes corresponding to the different post-buckling stages. At the post-buckling stage, the position $\xi = 1$ corresponding to front of the half-wave of the initial buckling mode is transformed into the wave-valley of the next half-wave of the post-buckling mode, and then the half-wave of the post-buckling mode remains fixed in position and merely grows in amplitude. Therefore, the length $S_{t-\text{modulus}}$ of the first half-wave of

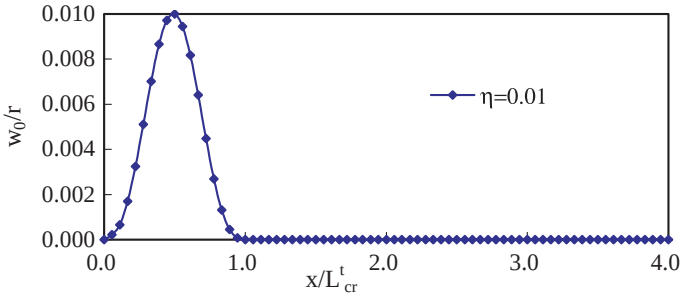

Fig. 3. Initial buckling mode of the aluminum-alloy bar B4.

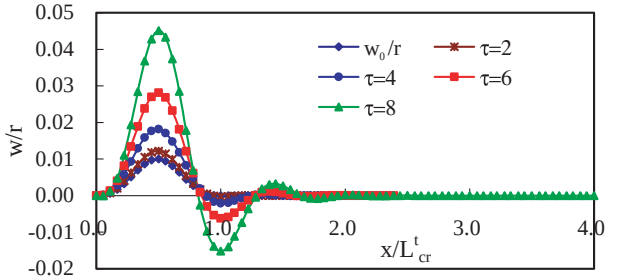

Fig. 4. Growth and spread of buckling deformation in the bar B4, $\eta = 0.01$.

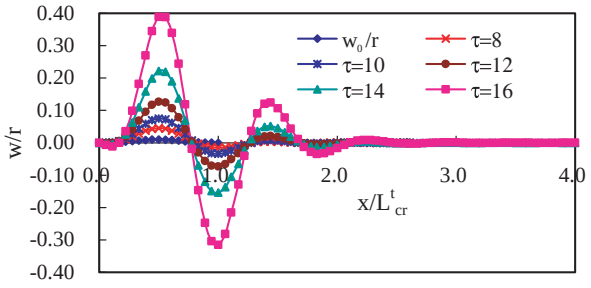

Fig. 5. Growth and spread of buckling deformation in the bar B4, $\eta = 0.01$.

the post-buckling mode is shorter than the half wavelength L^t_{cr} of the initial buckling mode. From the data in Table 1, it will be seen that the values of $S_{t-\text{modulus}}$ are close to the half wavelength S_{exp} observed in the experiment of Lindberg and Florence (1983).

The influence of the amplitude parameter η of the initial buckling deflection $\bar{w}_0$ on the post-buckling deflection is shown in Fig. 6. From Fig. 6, it will be seen that, at a given instant $\tau = t/t^t_{cr}$, the amplitude of the post-buckling deflection is affected by the parameter η to a large extent, but the value of the parameter η almost has no influence on the waveform of the post-buckling deflection profile. Figs. 4–6 show that, at the post-buckling stage, the post-buckling deformation is still limited to a very short region near the impact end in comparison with the length of the bar, which is in agreement with the experimental results of Lindberg and Florence (1983) (see Fig. 2.23 in Lindberg and Florence, 1983).

At the several different instants of the post-buckling stage, the average axial stress at the cross-section of the bar B4, due to the propagation of the elastic and plastic compression waves, is shown in Figs. 7–9. As shown in Figs. 7 and 9, the axial compression stress in the region covered by the elastic and plastic compression waves increases with the time until the instant $\tau = 10$. In comparison, the increase of the stress in the region covered by the plastic wave is more obvious. From Figs. 8 and 9, it is found that the perceptible unloading of the axial compression wave appears in the region near the impacted end after the instant $\tau = 12$, and the amplitude of unloading and the length of the unloading region increase with the growth of he post-buckling deflection.

At the several different stages of the post-buckling process, the maximum bending stress at the cross-section of the bar B4, related to the post-buckling deflection, is shown in Fig. 10. From the comparison between Figs. 9 and 10, it will be seen that the appearance of the bending stress is limited a narrow region near the impact end, and amplitude of the bending stress is small in comparison with the axial stress at this stage.

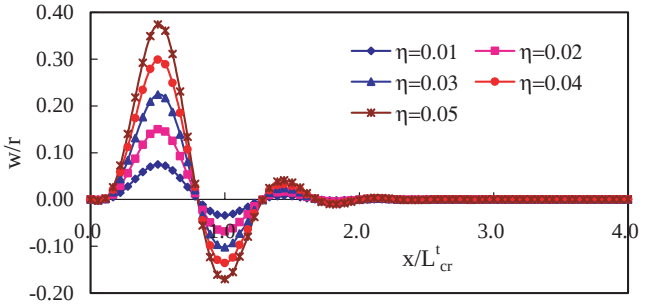

Fig. 6. The influence of the amplitude parameter on the post-buckling deflection profile, $t/t^t_{cr} = 11$.

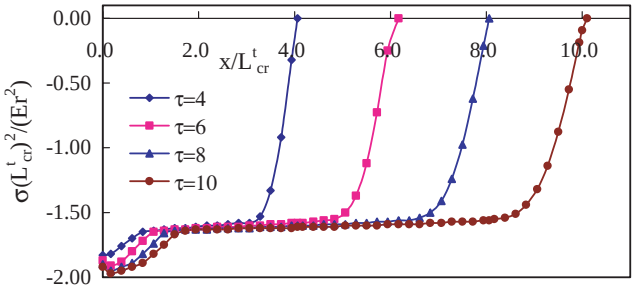

Fig. 7. Axial stresses in the bar B4 at post-buckling stages, $\eta = 0.01$.

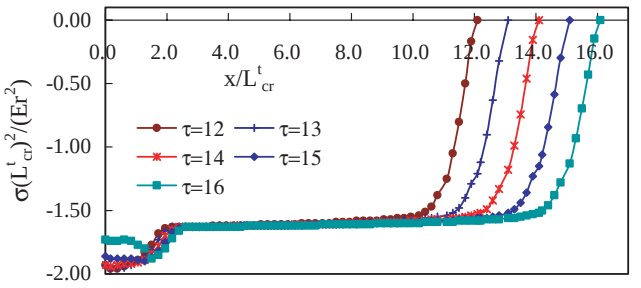

Fig. 8. Axial stresses in the bar B4 at post-buckling stages, $\eta = 0.01$.

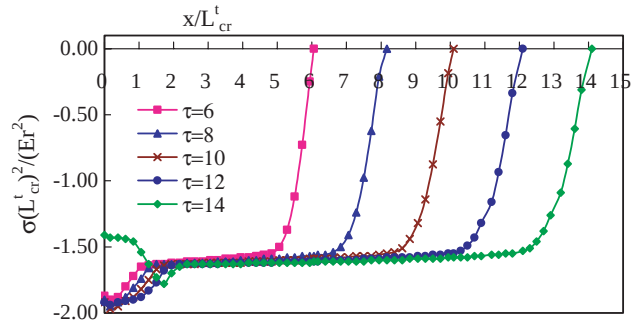

Fig. 9. Axial stresses in the bar B4 at post-buckling stages, $\eta = 0.03$.

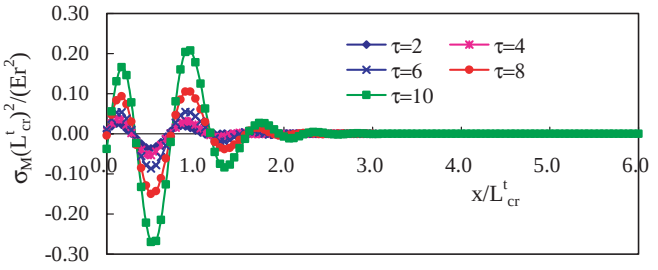

Fig. 10. Bending stresses in the bar B4 at post-buckling stages, $\eta = 0.03$.

To examine the validity of the tangent-modulus theory for describing the relation between the bending-moment and curvature in the dynamic plastic post-buckling deformation, the increments of the average axial stress and the maximum bending stresses corresponding to the time increment $\Delta\tau = 1$ at the different post-buckling stages are calculated, and the comparison is shown in Figs. 11–16. From Figs. 11–13 and 16, it will be seen that, at every cross-section in the region where the bending stress is produced due to the buckling deformation, the amplitude of the axial compressive-stress increment is larger than the increment of the maximum bending stress for the post-buckling stage corresponding to the duration from $\tau = 1$ to $\tau = 10$. Therefore, at this stage, no strain-rate reversal occurs in the bar and the solution corresponding to the tangent-modulus theory is valid for the dynamic plastic post-buckling response.

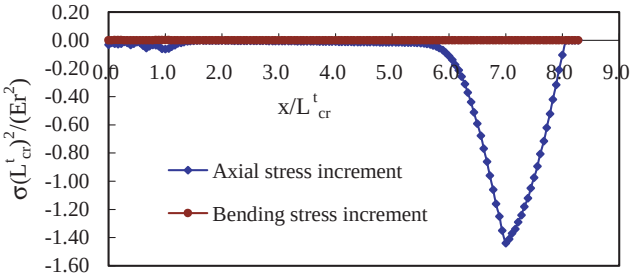

Fig. 11. The increments of axial stress and bending stress corresponding to the time increment from $\tau = 7$ to $\tau = 8$ for Specimen B4, with $\eta = 0.01$.

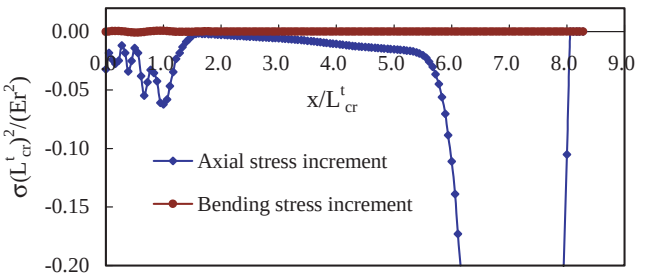

Fig. 12. The increments of axial stress and bending stress corresponding to the time increment from $\tau = 7$ to $\tau = 8$ for Specimen B4, with $\eta = 0.01$.

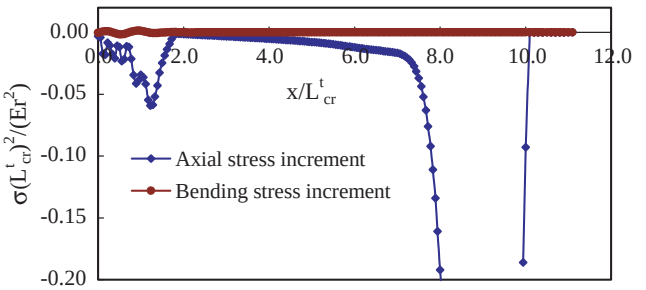

Fig. 13. The increments of axial stress and bending stress corresponding to the time increment from $\tau = 9$ to $\tau = 10$ for Specimen B4, with $\eta = 0.01$.

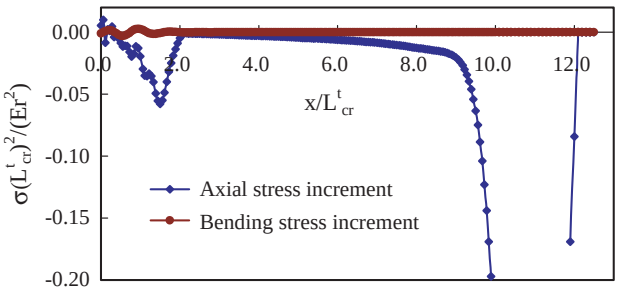

Fig. 14. The increments of axial stress and bending stress corresponding to the time increment from $\tau = 11$ to $\tau = 12$ for Specimen B4 , with $\eta = 0.01$.

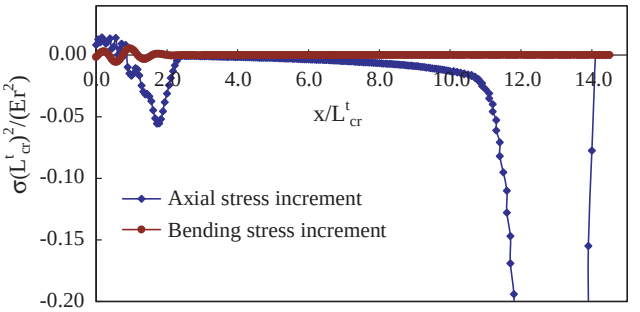

Fig. 15. The increments of axial stress and bending stress corresponding to the time increment from $\tau = 13$ to $\tau = 14$ for Specimen B4, with $\eta = 0.01$.

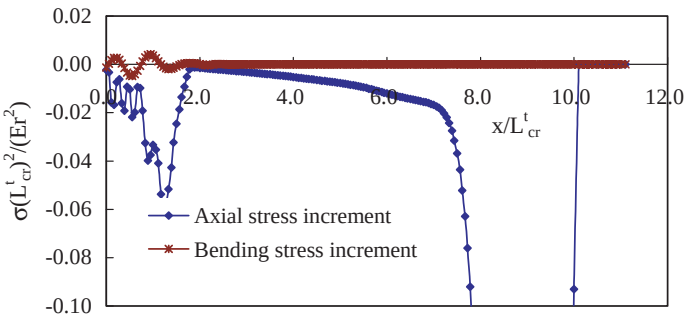

Fig. 16. The increments of axial stress and bending stress corresponding to the time increment from $\tau = 9$ to $\tau = 10$ for Specimen B4, with $\eta = 0.03$.

After the instant $\tau = 12$, the unloading of the axial compression waves appears in the region near the impact end and the unloading region extends towards the inside of the bar with the growth of the buckling deformation, as shown in Figs. 14, 15, 8 and 9. In the unloading region, where strain reversal takes place on the convex side of the bar, the bending stiffness of the bar increases, becoming partly governed by the elastic modulus E. For this part of the bar, the application of the tangent-modulus theory will result in that the

computed bending stiffness is smaller than the actual stiffness and the computed buckling deflection is larger than the actual. Considering that in Eqs. (4.5a–d) both loading and unloading cases of the axial stress are taken into account, the present solution developed by use of the tangent-modulus theory still can be applied to determining qualitatively the post-buckling behaviors of the bar after strain reversal occurrence.

5.2. The numerical results computed from the double-modulus theory

The values of the critical length L^r_{cr} and the critical time t^r_{cr} related to the first dynamic buckling mode, computed from the double-modulus theory, are list in the sixth and seventh columns of Table 1, respectively. For the bar B4, $L^r_{cr} = 44.05$ mm, $t^r_{cr} = 8.81 \times 10^{-6}$ s, and the elastic compression wave arrives at the free end when $\tau = t/t^r_{cr} = 10.37$.

For the bar B4, the growth of the buckling deflection w with the time parameter τ, calculated by use of the double-modulus theory, is illustrated in Fig. 17. From the Figs. 4, 5 and 17, it will be seen that, from the double-modulus theory, we obtain the same buckling-growth pattern as that computed by use of the tangent-modulus theory.

At the several different instants of the post-buckling stage, the axial stress in the bar B4, computed by use of the double-modulus theory, is shown in Figs. 18 and 19. Fig. 18 illustrates the same loading phenomenon of the axial compression waves as that in Figs. 7 and 9, for the earlier stage of the post-buckling process. If we lengthen the bar, the unloading phenomenon of the axial compression waves will be discovered again from the calculation by use of the double-modulus theory, as shown in Fig. 19, which appears in the local region near the impact end after the instant $t/t^t_{cr} = 12$.

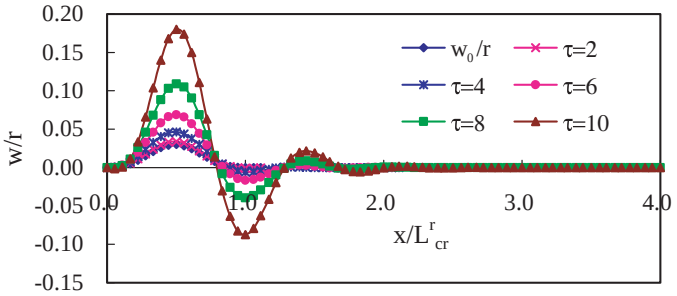

Fig. 17. Growth and spread of buckling deformation in the bar B4, with the double-modulus theory used and $\eta = 0.03$.

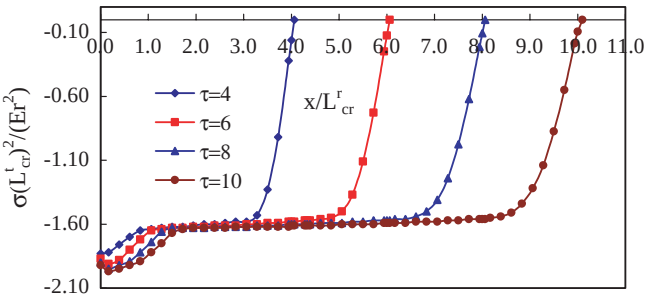

Fig. 18. Axial stress in the bar B4 at post-buckling stages, with the double-modulus theory used and $\eta = 0.03$.

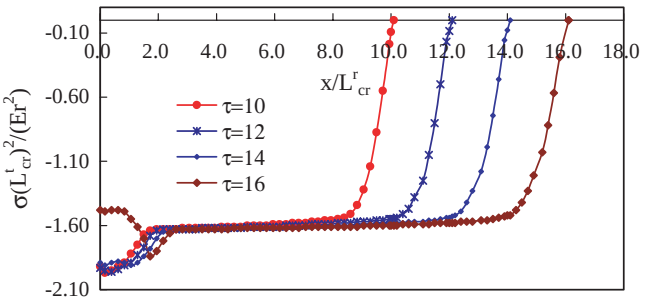

Fig. 19. Axial stresses in the bar B4 at post-buckling stages, with the double-modulus theory used and $\eta = 0.03$.

6. Conclusion

In order to clarify the developmental mechanism of the local plastic buckling and the interaction between the axial wave and the buckling deformation in an axially impacted slender-bar, the initial plastic local-buckling deflection, with a small amplitude parameter, obtained by the characteristic-value analysis is taken as the initial condition of the solution for the dynamic post-buckling response, instead of the initial imperfection distributed along the entire bar that is assumed in the literatures. The non-linear dynamic equations in the incremental form are derived and solved by use of the finite difference method, with the axial wave front treated as a moving boundary.

It is assumed that the bar is made of the linear strain-hardening material. The tangent-modulus theory and the double-modulus theory are applied, respectively, for describing the relation between the bending-moment and curvature in the plastic post-buckling deformation. In the relation between the axial stress-increment and strain-increment, both the loading case due to the compressive-wave propagation and the unloading case caused by the buckling deformation are taken into account. The validity of the theory is examined carefully by the numerical investigation.

The investigation results show that the initial buckling deformation with one half-wave, which occurs near the impact end at the critical instant, develops into the higher post-buckling mode with several half-waves, as the axial elastic and plastic compression waves propagate forward in the impact process. The position corresponding to the half-wave front of the initial mode is transformed into the wave-valley of the next half-wave of the higher post-buckling mode, so that the length of the first half-wave of the post-buckling mode is shorter than the half-wave length of the initial mode. The post-buckling deformation is still limited to a very short region near the impact end in comparison with the length of the bar, which is in agreement with the experimental results of Lindberg and Florence (1983).

At the early stage of the pot-buckling process, the average axial-compression-stress at the cross-section in the region covered by the elastic and plastic compression waves increases with the propagation of the compression waves towards the free end. When the post-buckling deflection develops large enough in the local region near the impact end, the unloading of the axial compression wave appears in this region and the unloading region extends towards the inside of the bar with the growth of the post-buckling deformation.

The bending stress produced due to the buckling deformation is limited a narrow region near the impact end for the slender bar under the axial high-velocity impact. Before the unloading of the axial compression wave occurs, the increment of the average axial-compression-stress at the cross-section, corresponding to a time increment Δt, exceeds the increment of the maximum bending stress computed from the tangent-modulus theory, so that no strain reversal occurs in the bar. Therefore, the present solution for the dynamic post-buckling response, corresponding to the tangent-modulus theory, is valid for the post-buckling stage

before appearance of the unloading of the compression wave. Considering that, in the non-linear dynamic equations, both loading and unloading cases of the axial compression waves are taken into account, the solution still can be applied to determining qualitatively the dynamic post-buckling behaviors of the bar after appearance of the unloading of the axial compression wave.

Acknowledgement

This work is supported by grant No. 10272114 of National Natural Science Foundation of China.

References

Abrahamson, G.R., Goodier, N.J., 1966. Dynamic flexural buckling of rods within an axial plastic compression wave. J. Appl. Mech. 32, 241–247.

Bleich, F., 1952. Buckling Strength of Metal Structures. McGraw-Hill Book Company, Inc., New York.

Hayashi, T., Sano, Y., 1972a. Dynamic buckling of bars; 3rd report. In the case of elastoplastic bars. Bulletin of JSME 15, 1333–1338.

Hayashi, T., Sano, Y., 1972b. Dynamic buckling of elastic bars; 2nd report; the case of high velocity impact. Bulletin of JSME 15, 1176–1184.

Jones, N., 1989. Structural Impact. Cambridge University Press, Cambridge.

Karagiozova, D., Jones, N., 1996. Dynamic elastic–plastic buckling phenomena in a rod due to axial impact. Int. J. Impact Eng. 18, 919–947.

Lee, L.H.N., 1981. Dynamic buckling of an inelastic column. Int. J. Solids Struct. 17, 271–279.

Lepik, Ü., 2001. Dynamic buckling of elastic–plastic beams including effects of axial stress waves. Int. J. Impact Eng. 25, 537–552.

Lindberg, H.E., Florence, A.L., 1983. Dynamic pulse buckling-theory and experiment, Defence Nuclear Agency, Washington, Contract No. DNA 001-78-0287; Martinus Nijhoff, Norvell, MA, 1987.

Simitses, G.J., 1987. Instability of dynamically-loaded structures. Appl. Mech. Rev. 40, 1403–1408.

Simitses, G.J., 1989. Dynamic Stability of Suddenly Loaded Structures. Springer, New York.

Wang, A., Tian, W., 2002. Twin-characteristic-parameter solution for dynamic buckling of columns under elastic compression wave. Int. J. Solids Struct. 39, 861–877.

Wang, A., Tian, W., 2003a. Characteristic-value analysis for plastic dynamic buckling of columns under elastoplastic compression waves. Int. J. Non-Linear Mech. 38, 615–628.

Wang, A., Tian, W., 2003b. Twin-characteristic-parameter solution of axisymmetric dynamic plastic buckling for cylindrical shells under compression waves. Int. J. Solids Struct. 40, 3157–3175.

Wang, A., Tian, W., 2005. Twin-characteristic-parameters analysis for elastic dynamic buckling of thin cylindrical shells under axial step loading. Int. J. Impact Eng. 31, 643–666.

Wang, A., Tian, W., in press. Mechanism of buckling development in elastic bars subjected to axial impact. Int. J. Impact Eng.